Tikrit Journal of Engineering Sciences (2025); 32(4): 2121
DOI: http://doi.org/10.25130/tjes.32.4.22

IRAQI Academic Scientific Journals

ISSN: 1813-162X (Print); 2312-7589 (Online)
Tikrit Journal of Engineering Sciences
available online at: http://www.tj-es.com

TJES Tikrit Journal of Engineering Sciences

Finite Element Analysis of a Permanent Magnet Brushed DC Motor Based on RMxprt/Maxwell 2D

Aula Ghazi Salim *, Amer Mejbel Ali
Electrical Department, Engineering College, Mustansiriyah University, Baghdad, Iraq.

Keywords:
FEA; Maxwell 2D; PMDC motor; Reverse engineering; RMxprt.

Highlights:

- *Hybrid FEM-Analytical method was proposed to analyze a PMDC motor.*
- *Back engineering was used to extract the design documents of PMDC motor.*
- *RMxprt and Maxwell software were adopted to obtain the simulation results of PMDC motor.*

ARTICLE INFO
Article history:

Received	06 Apr. 2024
Received in revised form	10 May 2024
Accepted	11 Dec. 2024
Final Proofreading	25 Aug. 2025
Available online	30 Aug. 2025

Citation: Salim AG, Ali AM. **Waste Rubber-Polyethylene Composite Materials for Enhancement of Mechanical, Thermal, and Electrical Properties–A Critical Review**. *Tikrit Journal of Engineering Sciences* 2025; **32**(4): 2121. http://doi.org/10.25130/tjes.32.4.22

**Corresponding author:*

Aula Ghazi Salim
Electrical Department, Engineering College, Mustansiriyah University, Baghdad, Iraq.

Abstract: This study presents a hybrid FEM-analytical methodology to analyze a permanent magnet-brushed DC (PMDC) motor. A test motor was selected as a trial example for powering a windshield wiper in an automobile, with specifications of 12 Volts, 50 Watts, and two poles. Reverse engineering was utilized by disassembling the motor and obtaining precise measurements of each component's dimensions. RMxprt and Maxwell 2D are both software tools and parts of the ANSYS Maxwell suite used for designing and analyzing electrical machines; however, they perform distinct functions. RMxprt focuses on initial design and parametric studies of electric machines, quickly assessing their impact on performance. At the same time, Maxwell 2D is suited for detailed electromagnetic field analysis, including fields, forces, mesh, flux, and more complex simulations, as well as motor performance analysis based on current, speed, and efficiency. They are used together to leverage their complementary strengths in the design and analysis workflow. The simulation results are compared with the experimental results, and the results were found to be convergent.

تحليل العنصر المحدد لمحرك تيار مستمر ذو مغناطيس دائم وفرشاة إستناداً إلى برنامج RMxprt/Maxwell 2D

غلا غازي سالم، عامر مجبل علي
قسم الهندسة الكهربائية /كلية الهندسة /الجامعة المستنصرية / بغداد – العراق.

الخلاصة
تقدم هذه الدراسة منهجية هجينة FEM- تحليلية لتحليل محرك تيار مستمر بفرش ومغناطيس دائم (PMDC) . تم اختيار محرك اختبار كمثال تجريبي لتشغيل ممسحة الزجاج الأمامي في سيارة، بمواصفات ١٢ فولت، ٥٠ واط، وقطبين. تم استخدام الهندسة العكسية من خلال تفكيك المحرك والحصول على قياسات دقيقة لأبعاد كل جزء فيه. RMxprt و Maxwell 2D كلاهما أدوات برمجية وأجزاء من مجموعة ANSYS Maxwell المستخدمة لتصميم وتحليل الآلات الكهربائية ، لكنهما يؤديان وظائف متميزة. يركز RMxprt على التصميم الأولي والدراسات البارامترية للآلات الكهربائية ويقيم بسرعة بتأثيرها على الأداء. في الوقت نفسه ، يُعد Maxwell 2D مناسبًا لتحليل المجال الكهرومغناطيسي المفصل، بما في ذلك المجالات والقوى والشبكة والتدفق والمحاكاة الأكثر تعقيدًا، فضلاً عن تحليل أداء المحرك بناء على التيار والسرعة والكفاءة. يتم استخدامها معًا للاستفادة من نقاط قوتها التكميلية في سير عمل التصميم والتحليل. تمت مقارنة نتائج المحاكاة مع النتائج التجريبية وكانت النتائج متقاربة.
الكلمات الدالة: تحليل العنصر المحدد (FEA)، Maxwell 2D، محرك تيار مستمر ذو مغناطيس دائم (PMDC)، الهندسة العكسية، RMxprt.

1.INTRODUCTION

Permanent magnet-brushed DC motors (PMDC) are commonly utilized in automobiles and factory automation systems. Medical devices and household appliances have a wide range of applications, and their demand is increasing as the automobile and control equipment industries grow [1]. For example, numerous applications are produced daily to simplify and enhance the user experience, such as controlling automobile windows and assisting with steering wheel functions. However, when designing such electric motors, the power source available on the application vehicle — typically DC — must be taken into consideration [2]. The low-voltage range, i.e., 12–24 V, is where permanent magnet-brushed DC motors are typically used, as shown in the economical auxiliary drive structures prevalent in automotive applications [3]. As a result, the DC electric motors are the most typical application. Numerous research studies have been conducted to obtain the design information for permanent magnet DC motors [2–6]. However, it relied on ready-made design information for the motors it studied. In contrast, the lack of this information characterizes the present study; however, it was extracted through reverse engineering. This work focused on simulating and analyzing a 50W, 12V PMDC motor used to operate a windshield wiper. The motor's performance will then be analyzed using RMxprt and Maxwell 2D software, and the results will be compared with the test results. The rest of this paper is organized as follows: Section 2 presents the basic equations and concepts of PMDC motor operation and analysis. Section 3 covers the modeling setup, simulation, and parameters of a permanent-magnet-brushed DC test motor used to operate car windshield wipers, describing the software tools used in the analysis. Section 4 presents and discusses the results from the Ansys-Maxwell suite, RMxprt, and Maxwell 2D. Also, Section 4 compares the present results with the experimental results to ensure the accuracy of the models used. Finally, Section 5 summarizes the main findings of the research.

2.MATHEMATICS OF THE PMDC MOTOR

The mathematical analysis of Permanent Magnet-Brushed DC motors (PMDC) entails understanding the various aspects that impact motor performance, including electrical, magnetic, and mechanical components. These motors operate by utilizing permanent magnets to generate a steady magnetic field. This field interacts with the conductors, delivering the current to produce torque. The fundamentals of PMDC motor mathematics include equations controlling electromagnetic principles, torque generation, and loss mechanisms [7, 8]. Motor performance and efficiency can be thoroughly analyzed and improved by examining these factors. This section will examine the fundamental equations and principles governing the operation and analysis of PMDC motors.

2.1.Formulas from the Equivalent Circuit of a PMDC Motor

The analogous circuit of the PMDC motor is shown in Fig. 1.

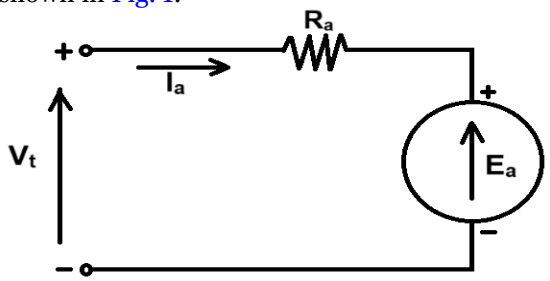

Fig. 1 Equivalent Circuit of the PMDC Motor.

The electric driving force and torque characteristics of the PMDC motor are identical to those of the weak-type DC motor and may be mathematically represented as [1]:

$$E_a = k\omega\Phi \quad (1)$$

$$T = k\Phi I_a \quad (2)$$

$$k = \frac{Zp}{2\pi a} \quad (3)$$

where Ea is the back emf, Ia is the armature current conductor, ω is the angular velocity

(rad/sec), Φ is the flux per pole, Z is the total number of armatures, p is the number of poles, a is the number of parallel paths in the armature, and k is the speed-volt constant or Torque constant. Equation (4) can be written from the equivalent circuit. The relationship between the developed and the load torque is shown in Eq. (5).

$$V_t = E_a + I_a R_a + V_b \quad (4)$$

$$T = J\frac{d\omega}{dt} + D\omega + T_l \quad (5)$$

where V_t is the terminal voltage, R_a is the armature winding resistance, V_b is the brush voltage drops, J is the moment of inertia (kg-m²), T is the developed motor torque (N. m), $\frac{d\omega}{dt}$ is the angular acceleration, D is the damping coefficient (N · m · s/rad), and T_l is the load torque (N · m).

2.2.Formulas for Finite Element Analysis

The equations proposed by James Clerk Maxwell explain the electromagnetic field. These include [1]:

$$\nabla \times H = J \quad (6)$$

$$\nabla \cdot B = 0 \quad (7)$$

$$B = \mu H \quad (8)$$

where B is Tesla's magnetic flux density, J is electric current density in (A/m2), H is magnetic field intensity in (A/m), and the scalar μ is permeability in H/m. There is a relationship between the magnetic flux density and the magnetic vector potential. The magnetic flux density and magnetic vector potential have the following relationship:

$$B = \nabla \times A \quad (9)$$

where A is called the vector potential for magnetism in (Wb/m). Since the intensity of magnetization of the permanent magnet PM is M, the internal equation of the permanent magnet PM will be:

$$B = \mu_0 H + M \quad (10)$$

The formula for torque as a function of the closed surface area can be obtained using Maxwell's method, as expressed in Eq. (11):

$$T = \frac{1}{\mu_0}\iint_s \left[(r \times B)(B \cdot n) - \frac{1}{2}B^2(r \times n)\right] dS \quad (11)$$

where r is the vector of the radius at the center of the rotor, n is the normal vector to the surface S, μ_o is the permeability of free space ($4\pi \times 10^{-7}$ N/A²), and ds is the vertical. The surface can be transformed into a charge amount in 2D analysis, as in Eq. (12):

$$T = \frac{1}{\mu_0}\oint_c r\, B_t\, B_r\, dC \cdot L \quad (12)$$

where B_r and B_t are two tangent and perpendicular components of the density of magnetic flux in the integral direction, and L is the Vector length (m).

2.3.Computation of DC Motor Losses

The motor power flow, illustrating the different losses of the PMDC motor, is shown in Fig. 2 [9, 10].

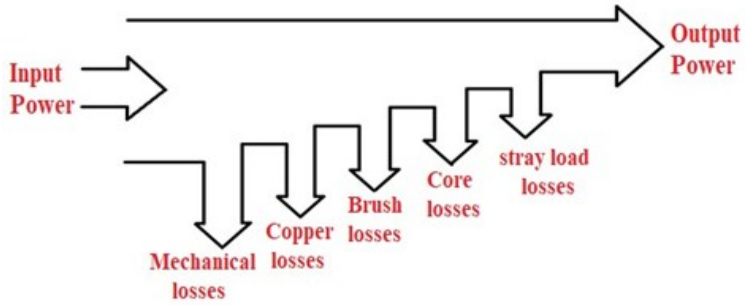

Fig. 2 Power Flow Diagram of a PMDC Motor

- **Copper losses P_{cu}**: Resistance in the motor's copper windings is the cause of copper losses. Heat dissipation is computed from these losses using Eq. (13) [16].

$$P_{cu} = RI^2 \quad (13)$$

where R is the motor windings' resistance, and I is the current passing through.

- **Brush drop losses P_B**: Brush drop loss refers to the loss of motor brush power across contact potential, as in Eq. (14).

$$P_B = V_{BD} I_a \quad (14)$$

where P_B = brush drop loss, V_{BD} = brush voltage drops, and Ia = armature current.
The computation of brush losses is based on the fact that the voltage drop across a set of brushes is generally consistent across a wide range of armature currents. Unless specifically mentioned, it is common to estimate the voltage decrease of the brush at 2 V [10, 11].

- **Mechanical losses P_{mech}**: The impact of mechanical forces causes mechanical losses in a DC motor. There are two fundamental categories of mechanical losses: friction and windage. Friction losses are caused by the motor's brushes, bearings, and other moving parts, whereas windage losses result from the air resistance the motor's spinning parts must overcome. The machine's bearings experience friction losses, while the moving parts of the machine rubbing against the air inside the motor's housing result in windage losses [10], as expressed by:

$$P_{mech} = T_f \omega \quad (15)$$

where T_f is friction torque (N · m), and ω is rotational velocity (rad/sec).

- **Core losses (P_{core}):** The motor's core losses comprise the metal's hysteresis and eddy current losses. Hysteresis losses occur due to the repeated magnetization cycles in the core material during rotor rotation and changes in the magnetic field. In contrast, eddy current losses are generated by currents induced in the core by changing magnetic fields. The losses experienced are directly proportional to the square of the flux density (B^2) and, in the case of the rotor, to the 1.6th power of the rotation speed ($n^{1.6}$) [10, 12, 14], as expressed by:

$$P_{core} = P_{hyst} + P_{eddy} \quad (16)$$

$$P_{hyst} = K_h f B^{1.6} \quad (17)$$

$$P_{eddy} = K_e f^2 B^2 \quad (18)$$

where P_{core} is the hysteresis loss (W/m^3), K_h is the hysteresis loss coefficient, P_{eddy} is the eddy current loss (W/m^3), K_e is the eddy current loss coefficient, B is the flux density amplitude within the material, and f is the applied excitation frequency, equal to the PMDC motors' electrical frequency, calculated from [13]:

$$f = pn * \frac{2\pi}{60} \quad (19)$$

where p is the number of pole pairs.

- **Stray losses P_{stray}**: The stray losses are considered to be 1% of the input power (p_{in}) [10], given by:

$$P_{stray} = 0.01 P_{in} \quad (20)$$

$$P_{in} = V I \quad (21)$$

where V is the applied voltage, and I is the input current.

Equation (22) calculates the electrical power input to a PMDC motor, which must equal the sum of the mechanical power output (P_{out}) and the total loss in the motor (P_l).

$$P_{in} = P_{out} + P_l \quad (22)$$

$$P_{out} = T_l \omega \quad (23)$$

$$P_l = P_{mech} + P_{cu} + P_{core} + P_B + P_{stray} \quad (24)$$

The motor's efficiency (η) can be represented as follows:

$$\eta = \frac{P_{out}}{P_{in}} * 100\% \quad (25)$$

3.MODELING OF THE PMDC MOTOR TESTED

A commercial, permanent-magnet, brushed DC test motor was used to operate automobile windshield wipers and is adopted as the test motor in this paper. The windshield wiper motor is shown in Fig. 3 (a). The cross-section of this motor is depicted in Fig. 3 (b).

3.1.Reverse Engineering

Reverse engineering was employed to obtain design information about this motor by disassembling it into its essential components, including the rotor, commutator, coils, and magnets, and measuring the dimensions of each component. Lap winding was used in the armature, with 42 conductors per slot. It has two brushes. The commutator consisted of 12 segments, 12 slots were equipped, and two parallel paths were in the armature winding. Fig. 3 (c) depicts the overall assembly of the test motor.

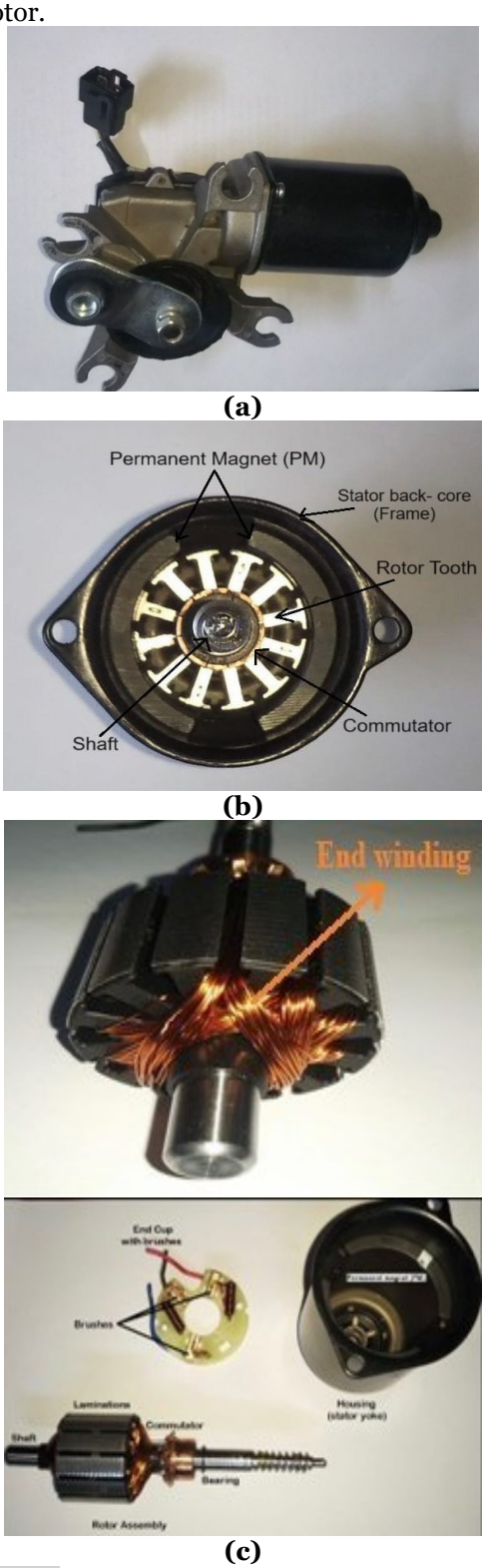

Fig. 3 Permanent Magnet-Brushed DC Test Motor.

3.2.Permanent Magnet-Brushed DC Motor Test Model

A permanent magnet-brushed DC motor test model was created to operate the windshield wipers, as shown in Fig. 4. Its purpose is to

measure the motor current and speed in all cases of load change. By calculating the current and speed values, the torque and input power were calculated, as shown in Table 1.

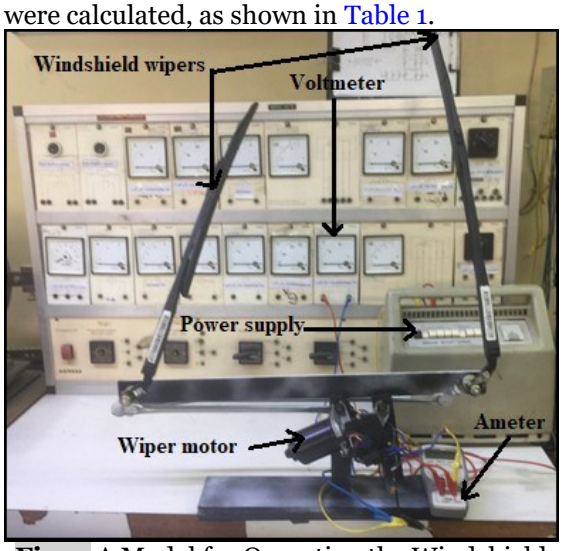

Fig. 4 A Model for Operating the Windshield Wipers.

Table 1 Test Results of Brushed PMDC Motor at Full-Load.

Parameter	Value	Unit
Current	6.42	A
Speed	1944	rpm
Torque	0.2456	N · m
Input power	77.04	W

3.3.Modelling and Simulation of The Tested PMDC Motor

Modeling, simulation, and analysis of motor performance were conducted using Ansys Maxwell and finite element analysis (FEM) in RMxprt. The software considered the parameters listed in Table 2 as input.

3.3.1.Motor Modeling by RMxprt

RMxprt is a template-based design tool in the Ansys-Maxwell suite used to build specialized machine design flows in response to the need for increased efficiency. RMxprt can compute machine performance, make preliminary sizing decisions, and conduct various evaluations using equivalent magnetic circuit techniques and classical analytical motor theory. It is possible to quickly compute key performance measures, such as torque versus speed, output power, input current, and efficiency. Geometry, materials, and boundary conditions may all be automatically set up for a Maxwell project (2D/3D) using RMxprt. The right symmetries, excitations, and coupling circuit topology make up the configuration for electromagnetic transient analysis [17]. Table 2 presents the analysis setup parameters for the design of the PMDC brush test motor.

Table 2 Experimental Motor Specifications.

Parameter	Value	Unit
Rated output power	50	w
Rated voltage	12	v
Rated speed	1944	rpm
Number of poles	2	

Figure 5 shows the stator model by RMxprt, and Table 3 shows the stator design parameters.

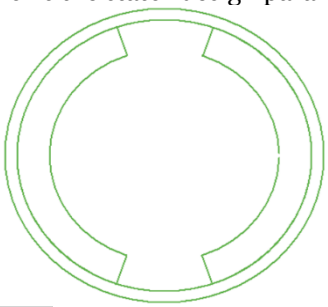

Fig. 5 Stator Model by RMxprt.

Table 3 Stator Design Parameters.

Parameter	Value	Unit
Stator Outer Diameter	56.6	mm
Stator Inner Diameter	41	mm
Stator Length	73.2	mm
Stator Stack factor	1	
Offset	0	mm
Steel Type (frame)	Steel_1008	
Embrace factor	0.786	
Magnet Type	Ceramic (ferrite) [15]	
Magnet Length	48.8	mm
Magnet Thickness	5.73	mm

Figure 6 shows the rotor lamination model by RMxprt, and Table 4 shows the rotor design parameters.

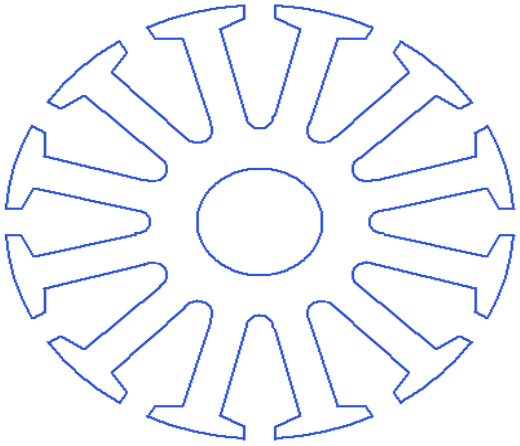

Fig. 6 Rotor Lamination Model by RMxprt.

Table 4 Rotor Design Properties.

Parameters	Value	Unit
Rotor Diameter (outer)	40	mm
Rotor Diameter (inner)	10	mm
Rotor Length	30	mm
Rotor Stack factor	0.95	
Rotor Types of steel	M600-50A	
Number of Slots	12	
Slot Insulation	0.33	mm
Conductors per Slot	42	
Coil Pitch	5	
Number of Wires per Conductor	2	
Wire Wrap	0.05	mm
Wire Diameter	0.5	mm
Skew Width	0	

Figure 7 and Table 5 show the dimensions of the rotor slot.

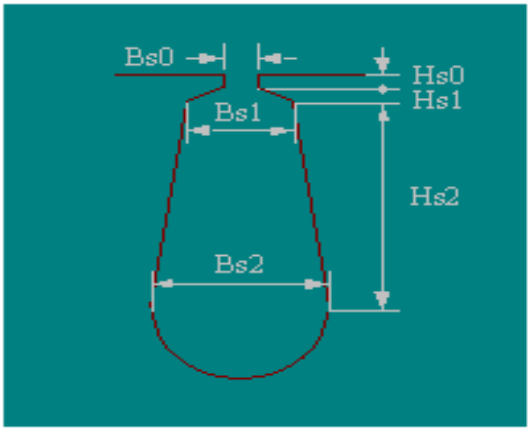

Fig. 7 Rotor Slot Type by RMxprt.

Table 5 Rotor Slot Diameters.

Parameters	Value	Unit
Hs0	1.2	mm
Hs1	1	mm
Hs2	8	mm
Bs0	2.5	mm
Bs1	6.4	mm
Bs2	2.4	mm

Figure 8 shows the test motor model by RMxprt, and Table 6 displays the commutator design parameters. The RMxprt models of the test motor are then exported to Maxwell 2D. This program produces meshes for FEA, and Maxwell 2D is used for electromagnetic analysis. Figure 9 depicts the Maxwell 2D motor model, and Figure 10 shows the finite element meshing of the test motor.

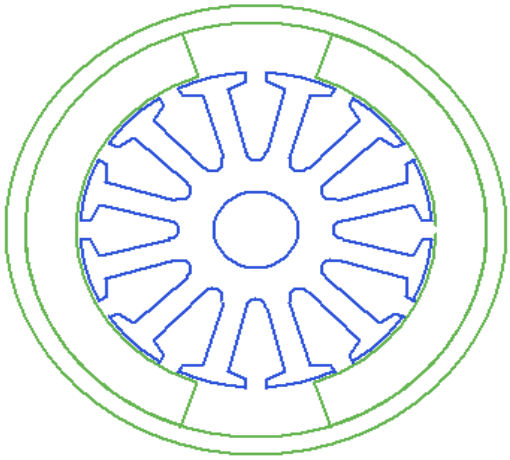

Fig. 8 PMDC Motor Model by RMxprt.

Table 6 Commutator and Brush Design Properties.

Parameters	Value	Unit
Commutator Type	Cylinder	
Commutator Diameter	18.3	mm
Commutator Length	12.2	mm
Commutator Insulation	0.2	mm
Brush Width	3.7	mm
Brush Length	9.7	mm
Brush Drop	1 [6]	v
Brush press	2 [13]	g/mm²
Frictional Coefficient	0.25 [13]	

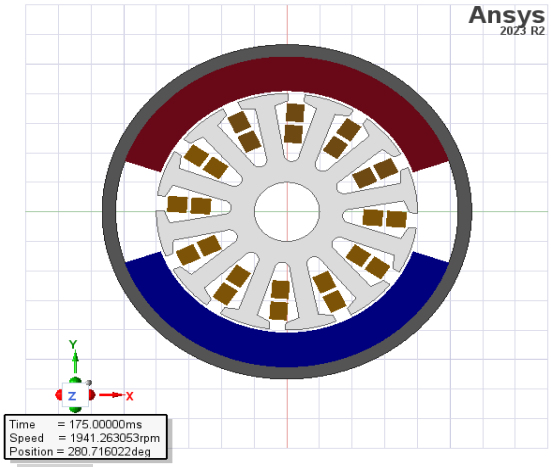

Fig. 9 2D Model Representation of a PMDC Motor by Maxwell 2D.

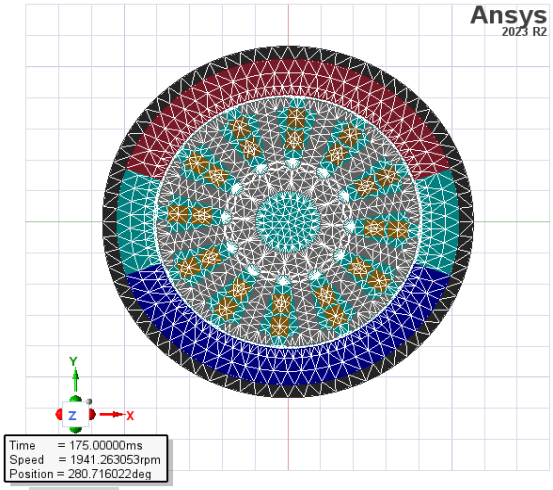

Fig. 10 The Meshing of the Test Motor by Maxwell 2D.

4.RESULTS AND DISCUSSION

This section presents and discusses the results obtained from the Ansys-Maxwell suite, including RMxprt and a finite element method based on Maxwell 2D, for the permanent magnet-brushed DC motor with a rating of 50W and 12V, 2 poles, and 12 slots. In RMxprt, the analysis focuses on calculating the main performance metrics and motor performance characteristics, as shown in Table 7 and Figures 11–14, respectively. In contrast, in Maxwell 2D, the analysis focuses on two cases: no load and full load, examining how to calculate performance metrics and their impact on motor performance, including torque, efficiency, and electromagnetic losses. The results are compared with the experimental results shown in the Tables (10–12) to ensure the accuracy of the models used.

4.1.RMxprt Results

After analyzing and simulating the PMDC motor in RMxprt, important data and curves were obtained. Table 7 represents the performance metrics of the test motor that RMxprt has calculated. Figure 11 illustrates the relationship between speed and torque, highlighting how torque decreases as speed

increases, indicating an inverse proportionality between speed and torque. At full load, the speed was 1908.51 rpm, and the torque was 0.2503 Nm. Figure 12 illustrates the relationship between the input current and the torque. The current directly increased with torque and decreased with increasing speed, resulting in a current value of 6.5395 A at full load and a torque of 0.2503 Nm. Figure 13 illustrates the relationship between the output power and torque, resulting in a power of 50,000 Watts at the rated speed and a torque of 0.2503 Nm. Figure 14 shows the variation of efficiency with torque in motor simulation, reaching 63.743% at rated speed and torque of 0.2503 Nm.

Table 7 Performance Metrics of the Test Motor by RMxprt

Parameter	Value	Unit
Speed at no-load	2699.51	rpm
Current at no-load	0.0831049	A
Input power at no-load	0.997259	W
Torque Constant KT	0.0387654	N · m/A
Cogging torque	0.0179656	N · m
Input current at full load	6.5395	A
Armature current at full load	3.26977	A
Windage Loss and Frictional	0.643854	W
Iron-core loss	1.02483e-05	W
Armature copper loss	21.2691	W
Brush loss	6.5395	W
Total loss	28.4525	W
Output power	50.022	W
Input Power	78.4745	W
Efficiency	63.743	%
Rated speed at full load	1908.51	rpm
Rated torque at full load	0.2503	N · m
Locked-rotor Torque	0.857397	N · m
Locked-rotor Current	22.1176	A

Figure 15 displays the typical performance characteristics of a PMDC motor.

4.2.Maxwell 2D Results

The FEM simulation was obtained by solving the test motor model using Maxwell2D.

- **At no-load:**

Figures 16–18 display the test motor torque, input current, and input power, respectively, as a function of time at no load. The no-load Maxwell 2D results can be summarized in Table 8.

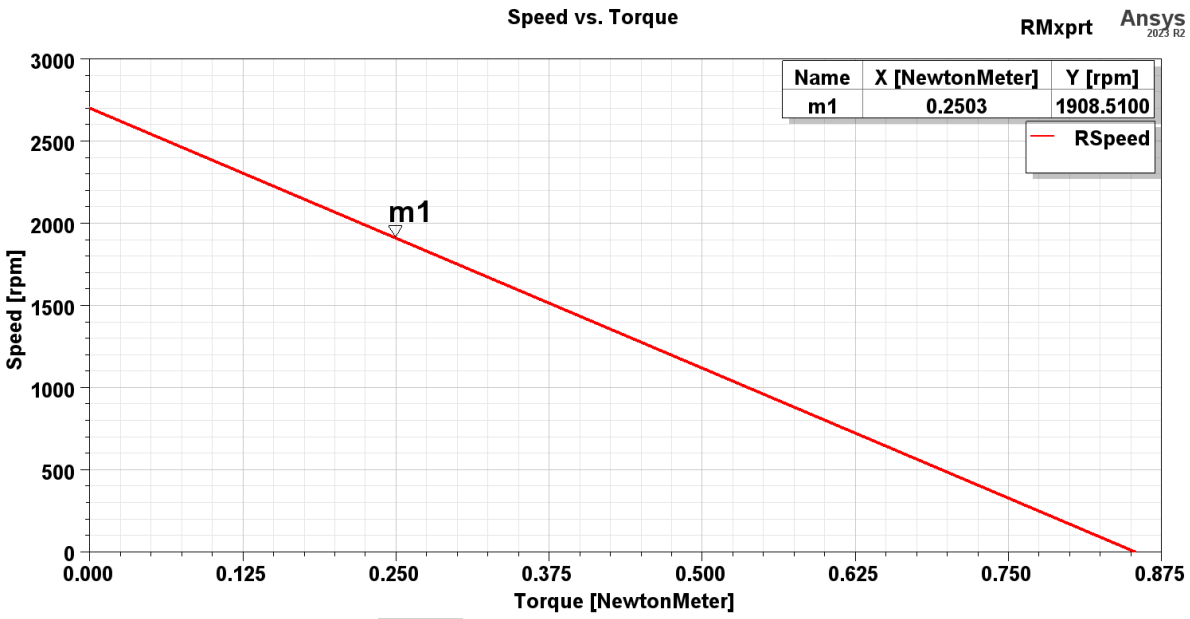

Fig. 11 Speed vs. Torque by RMxprt.

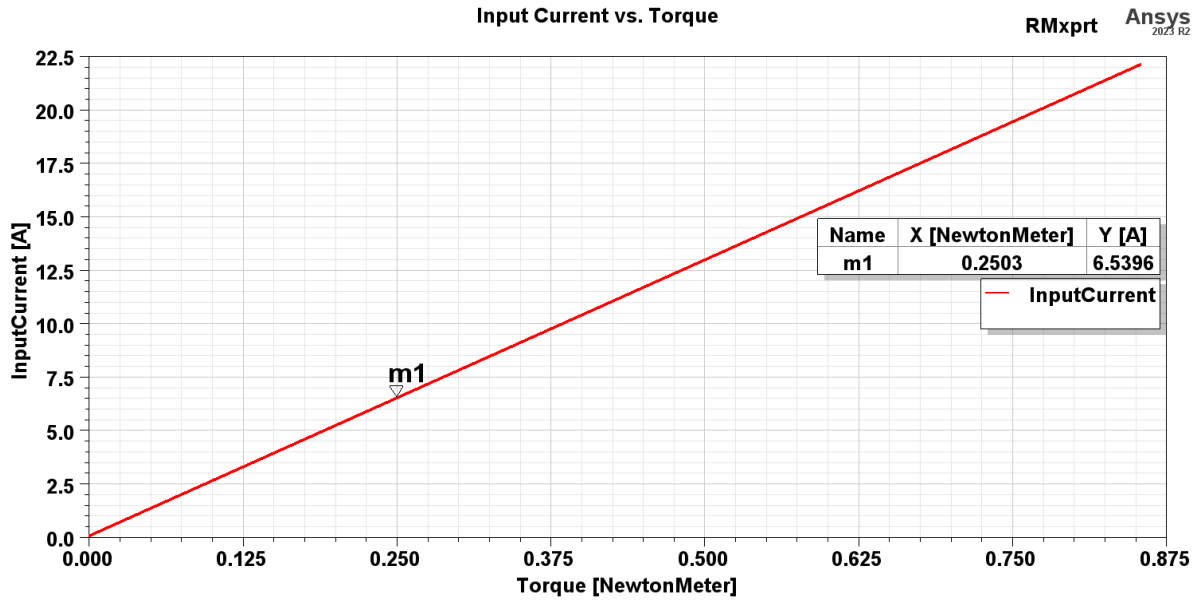

Fig. 12 Input current vs. Torque by RMxprt.

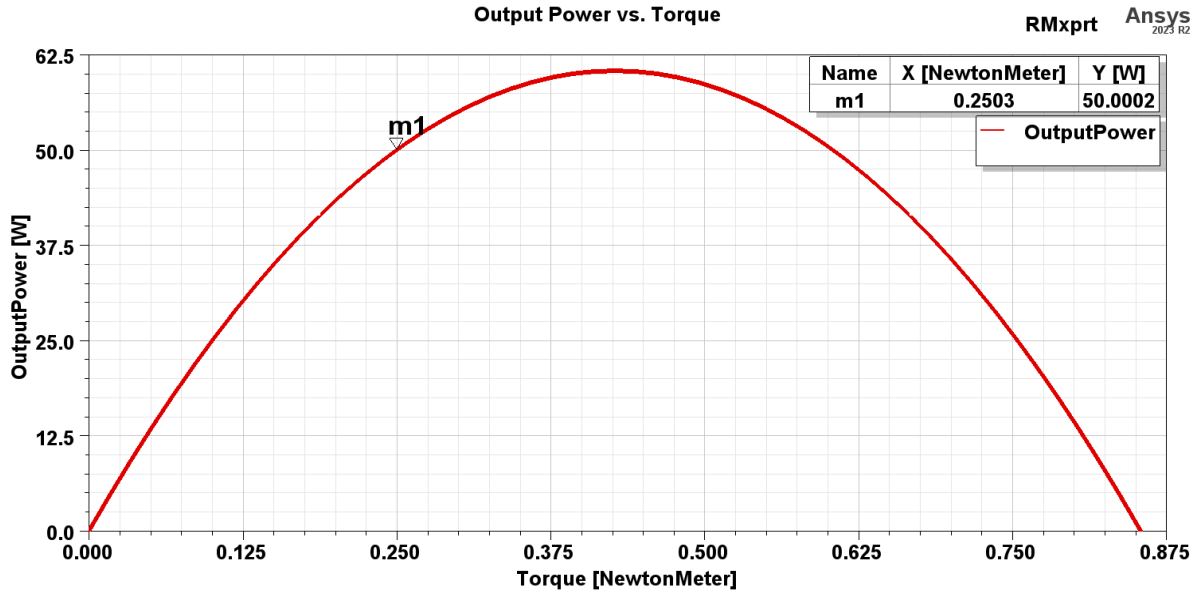

Fig. 13 Output Power vs. Torque by RMxprt.

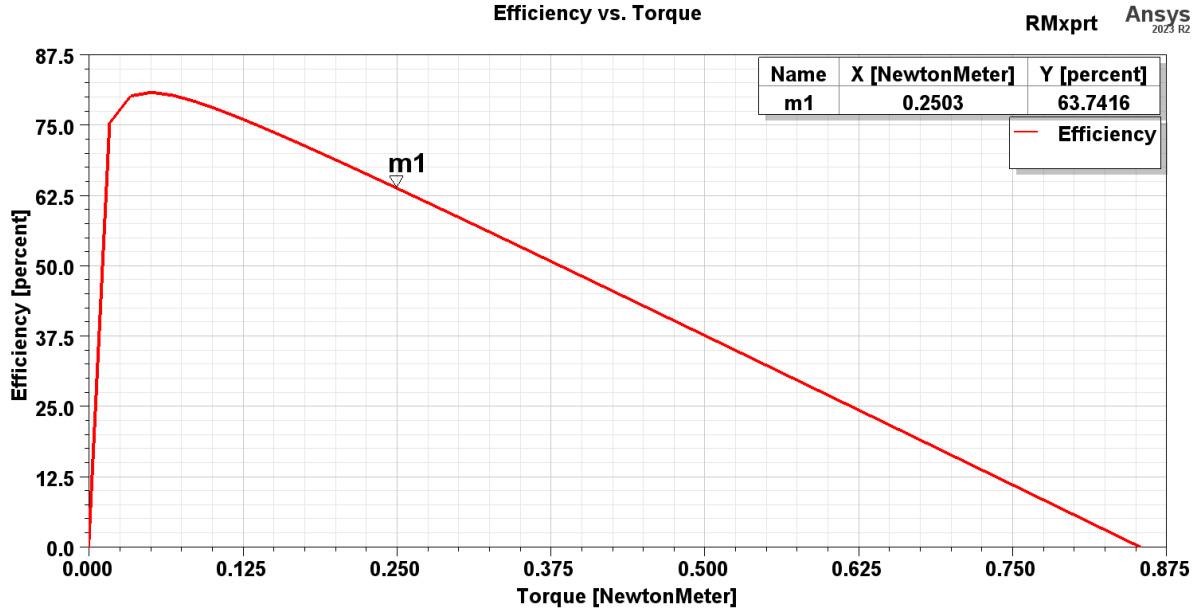

Fig. 14 Efficiency vs. Torque by RMxprt.

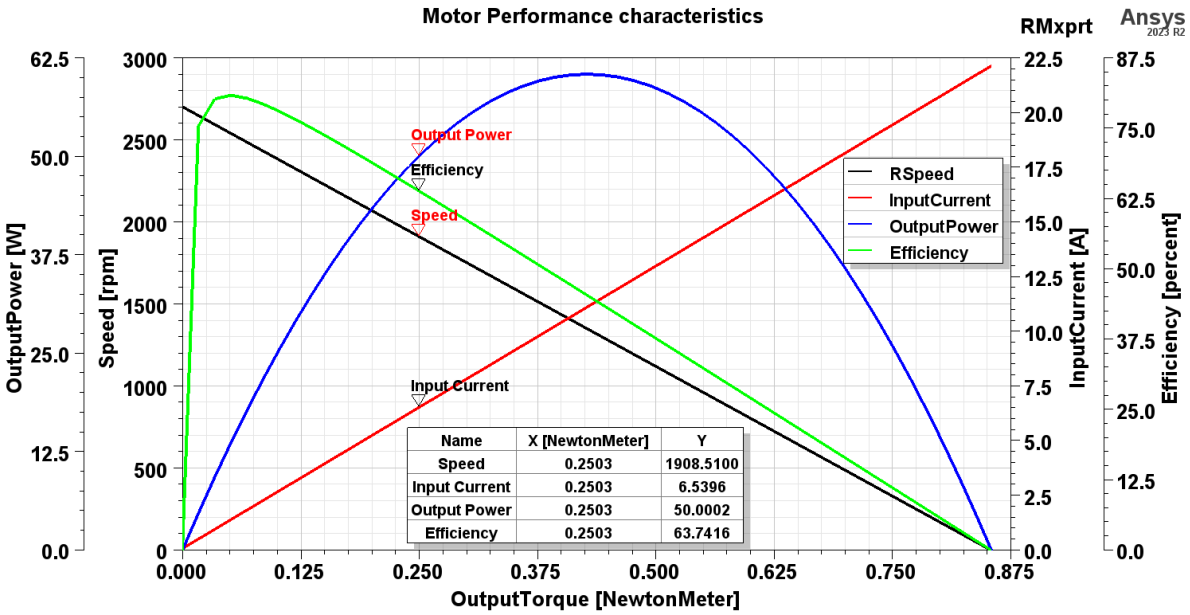

Fig. 15 Performance Curves of a PMDC Motor by RMxprt.

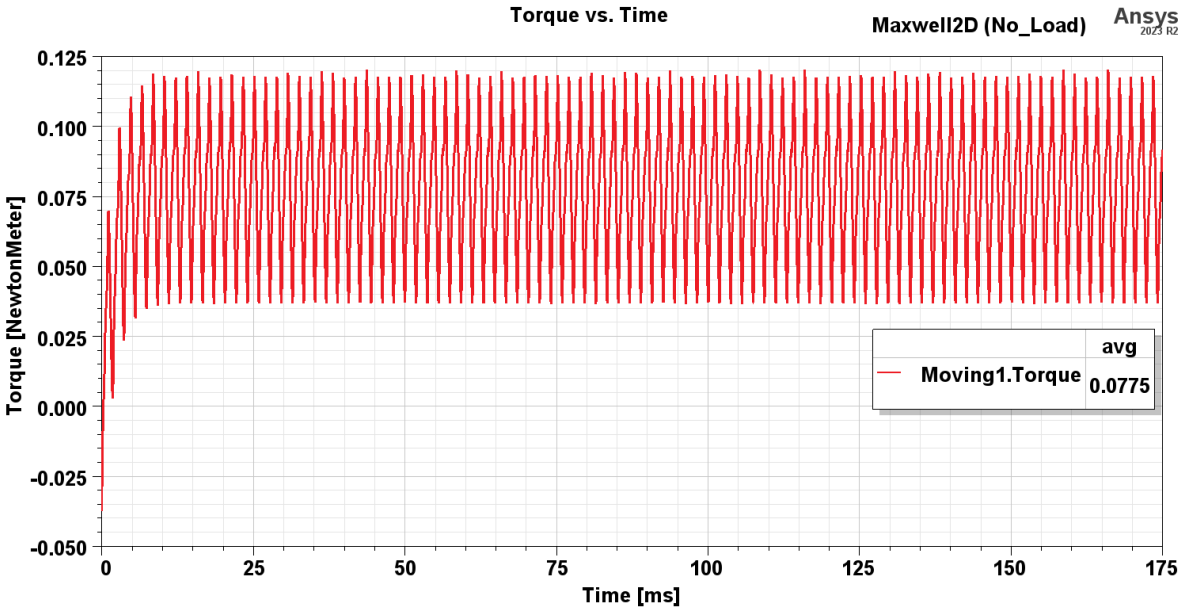

Fig. 16 PMDC Motor Torque at No-Load (speed= 2699.51 rpm) by Maxwell 2D.

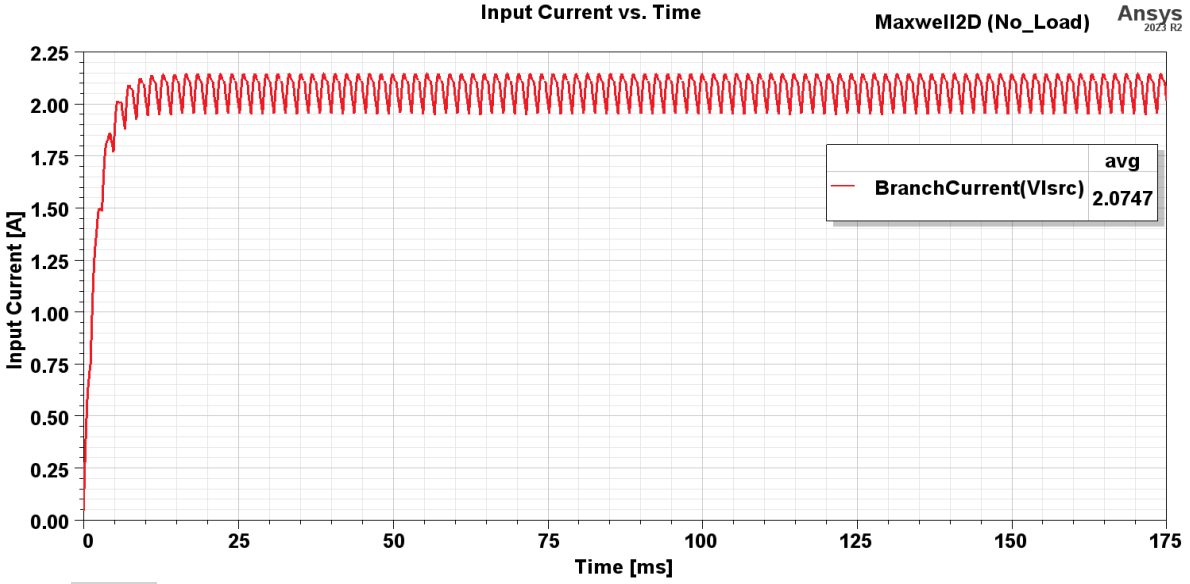

Fig. 17 Input Current of PMDC Motor at No-Load (speed= 2699.51 rpm) by Maxwell 2D.

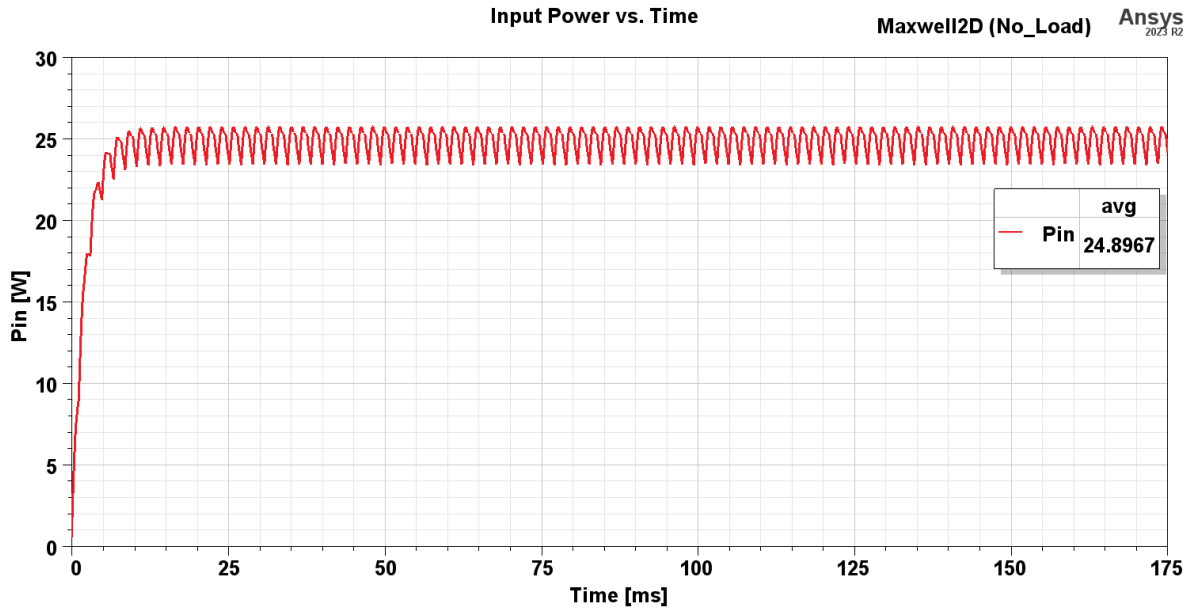

Fig. 18 Input Power of PMDC Motor at No-Load (speed= 2699.51 rpm) by Maxwell 2D.

Table 8 FEM Results by Maxwell 2D at No-Load.

Parameter	Value	Unit
Input Current	2.0747	A
Torque	0.0775	N · m
Input Power	24.8967	W

- **At full load,** the average value was calculated for the waveforms of speed, input current, torque, and input power. Additionally, the motor's efficiency was determined by computing its losses, i.e., copper, brush, mechanical, core, and stray losses, which were also computed using the average value of each wave. These results are displayed in Figures 19–22 below, which plot the average values of the waveform's speed, input current, torque, and input power versus time.

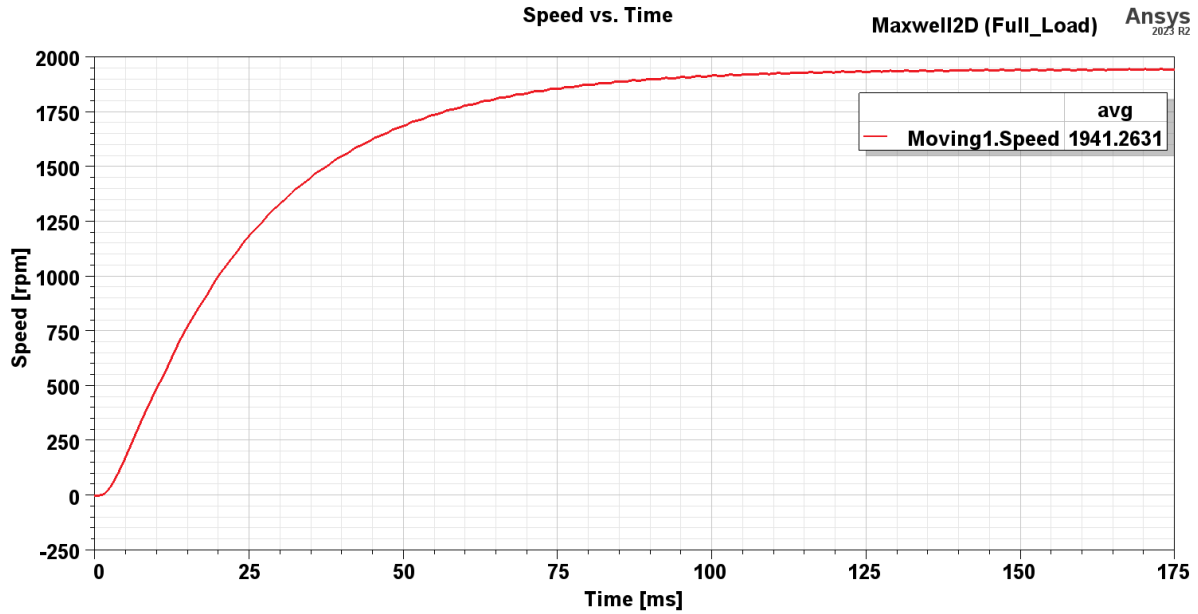

Fig. 19 Speed of PMDC Motor at Full Load by Maxwell 2D.

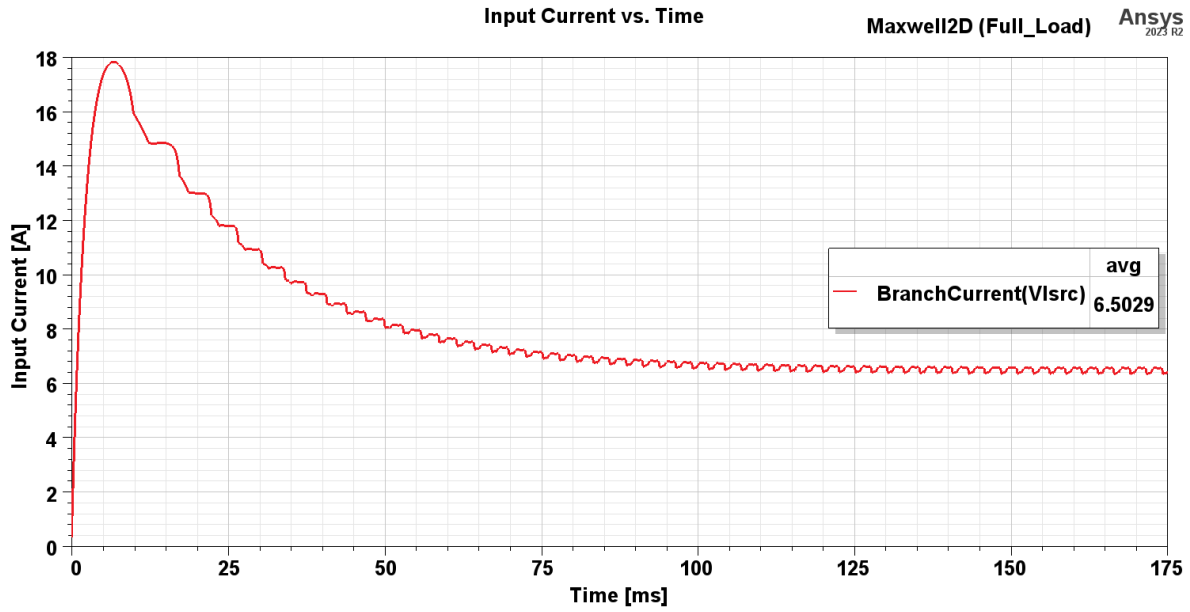

Fig. 20 Input Current of PMDC Motor at Full Load by Maxwell 2D.

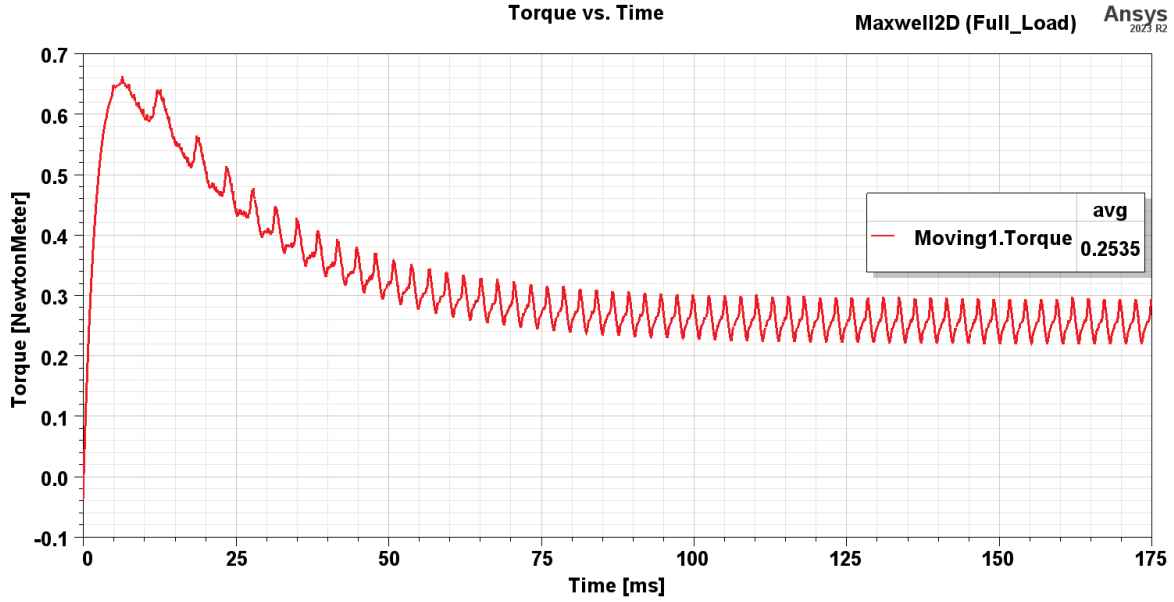

Fig. 21 PMDC Motor Torque at Full Load by Maxwell 2D.

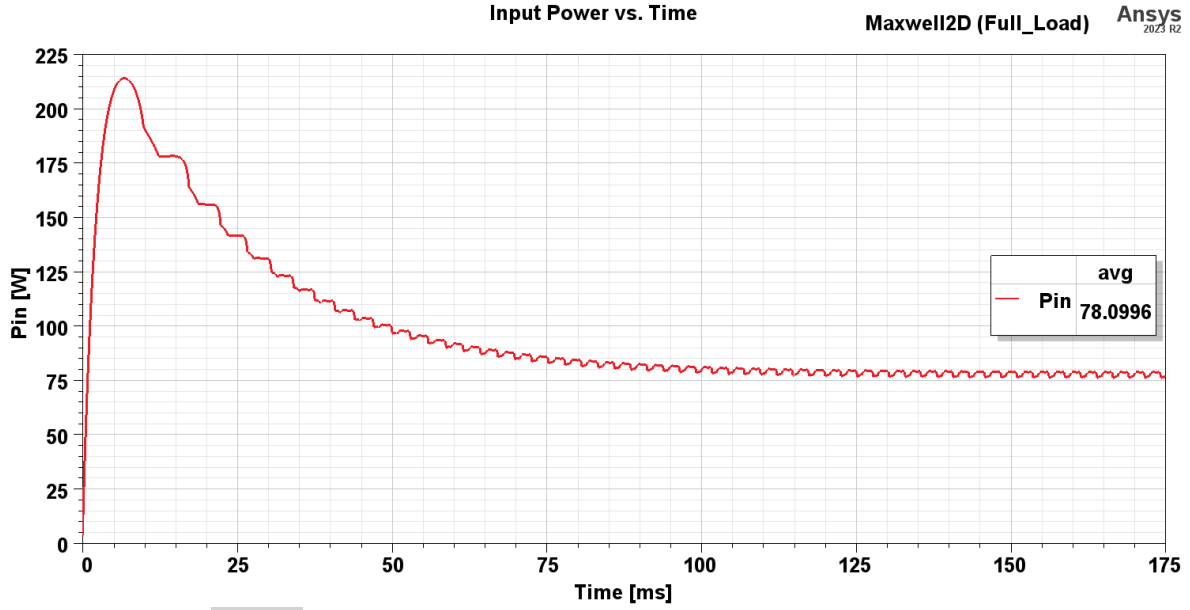

Fig. 22 Input Power of PMDC Motor at Full Load by Maxwell 2D.

Table 9 below lists the full-load simulation results calculated by Maxwell 2D.

Table 9 FEM Results at Full Load by Maxwell 2D.

Parameter	Value	Unit
Speed	1941.2631	rpm
Input Current	6.5029	A
Torque	0.2535	N · m
Input Power	78.0996	W

The calculation of motor efficiency by Maxwell 2D at full load involves the following steps:

1) Calculating motor output power (P_{out}), as shown in Fig. 23.
2) Calculating the armature copper loss (P_{cu}), as shown in Fig. 24.
3) Calculating the motor core losses, as shown in Fig. 25.
4) Calculating the motor Mechanical losses, as shown in Fig. 26.
5) Calculating the motor brush losses, as shown in Fig. 27.
6) Calculating the motor stray losses, as shown in Fig. 28.
7) Finally, motor efficiency was calculated by subtracting previous motor losses from the total power and then entering the result into the efficiency equation, as shown in Fig. 29.

Additionally, the FEM analysis of the test motor by Maxwell provides a clear illustration to motor designers of the magnetic flux distribution and magnetic field line distribution at various points in the motor model, as shown in Figs. 30 and 31. The error rate was calculated by comparing the experimental results with the simulation results from RMxprt and Maxwell 2D, and the findings are summarized in the tables below. Table 12 compares efficiency and losses computed in RMxprt and Maxwell 2D.

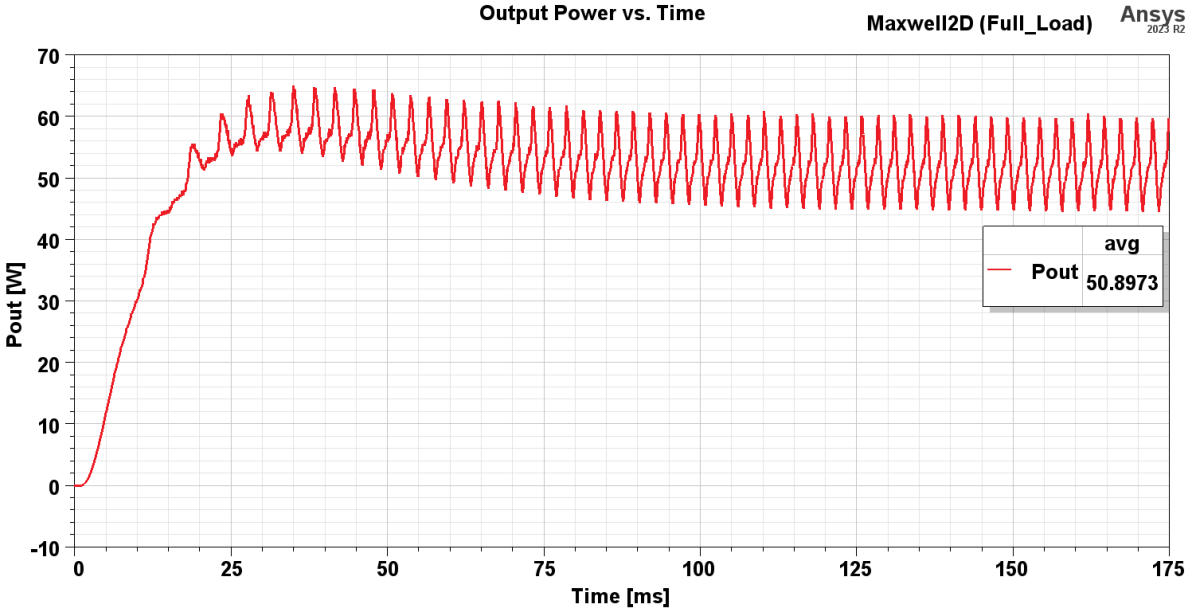

Fig. 23 Output Power of PMDC Motor at Full Load by Maxwell 2D.

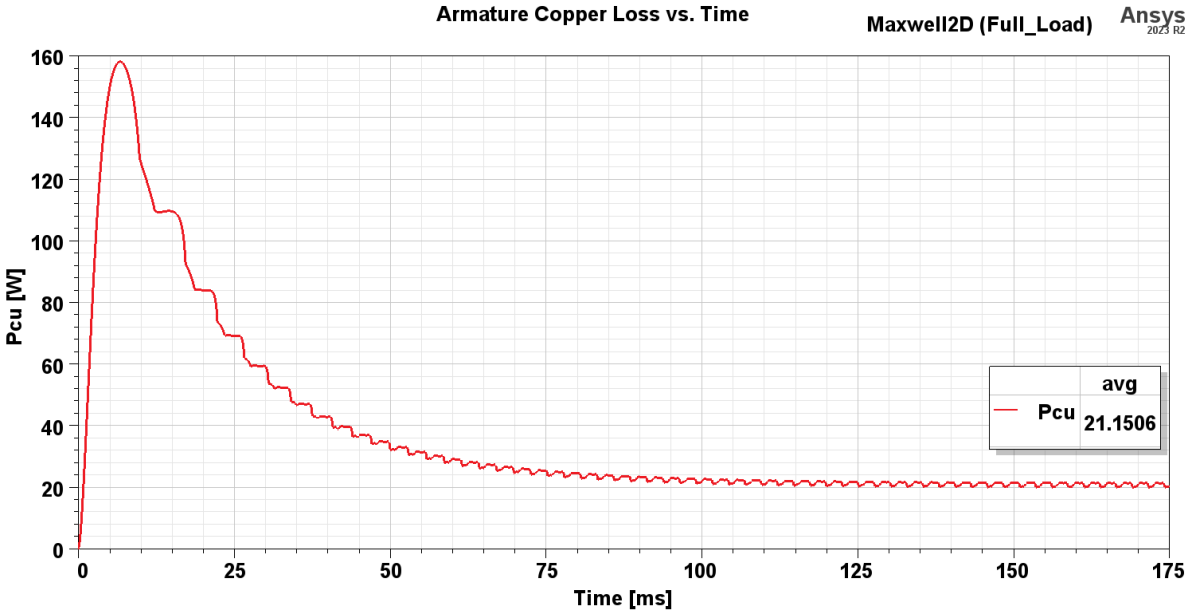

Fig. 24 Armature Copper Losses of PMDC Motor at Full Load by Maxwell 2D.

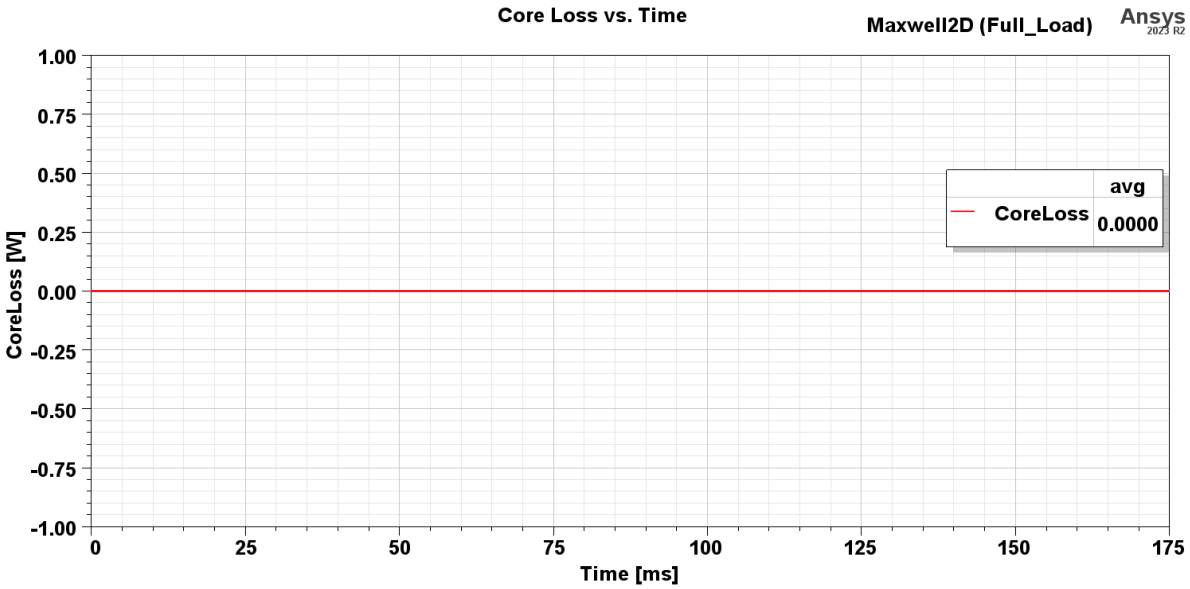

Fig. 25 Core Losses of PMDC Motor at Full Load by Maxwell 2D.

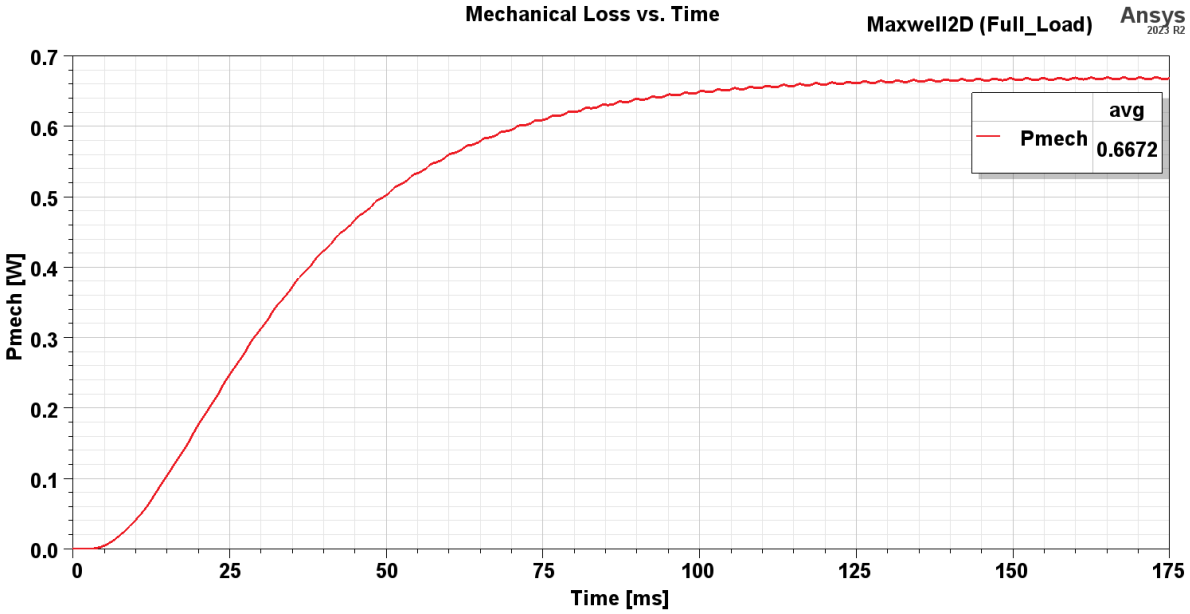

Fig. 26 Mechanical Losses of PMDC Motor at Full Load by Maxwell 2D.

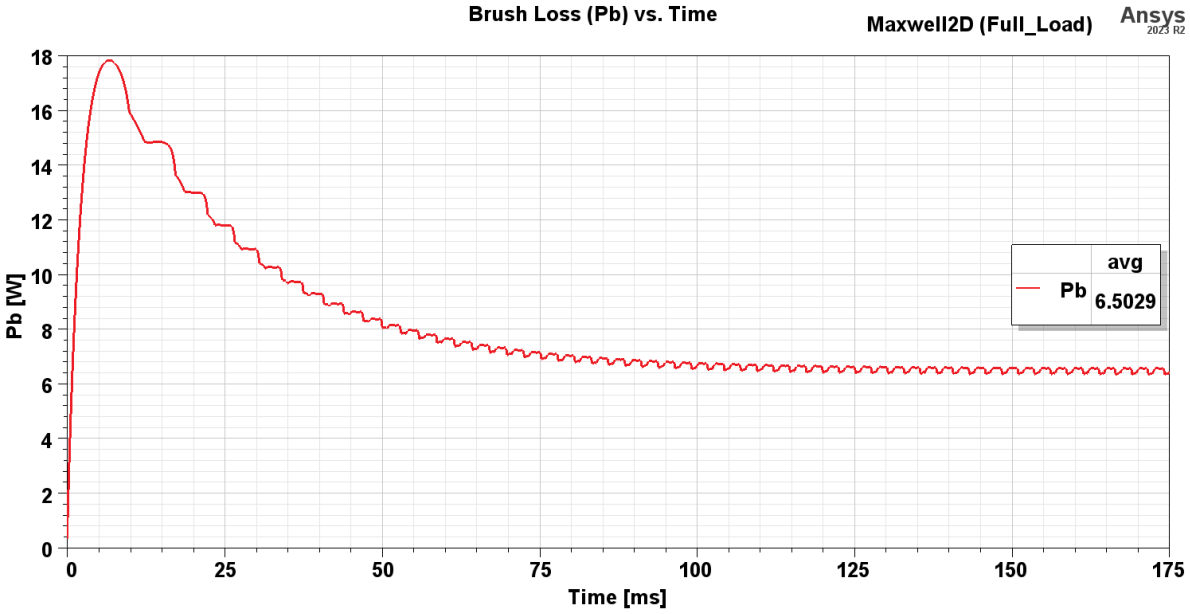

Fig. 27 Brush Losses of PMDC Motor at Full Load by Maxwell 2D.

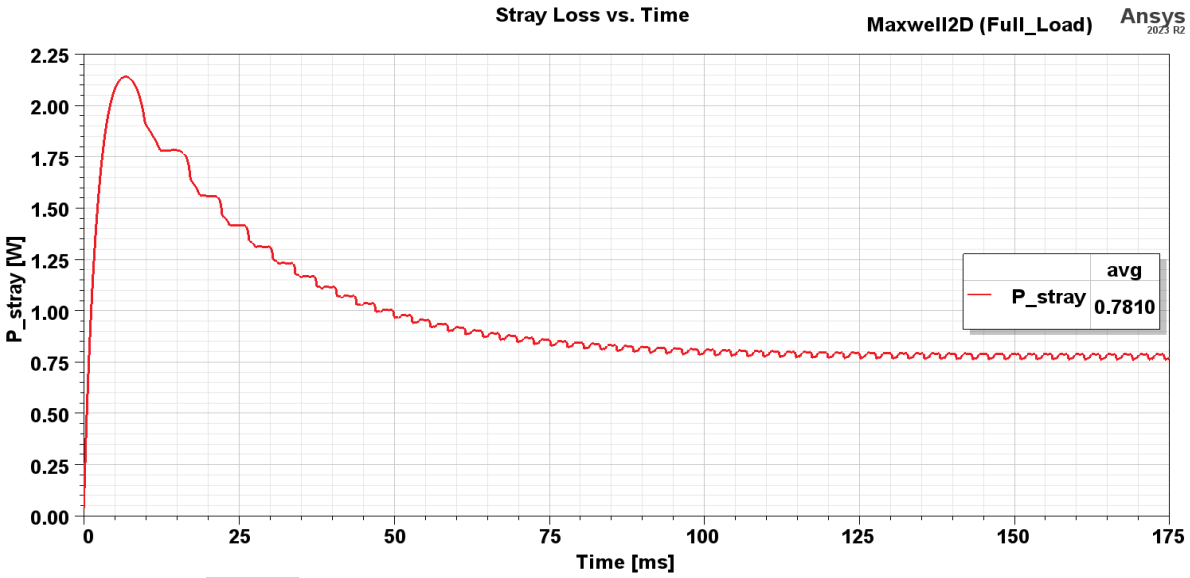

Fig. 28 Stray Losses of PMDC Motor at Full Load by Maxwell 2D.

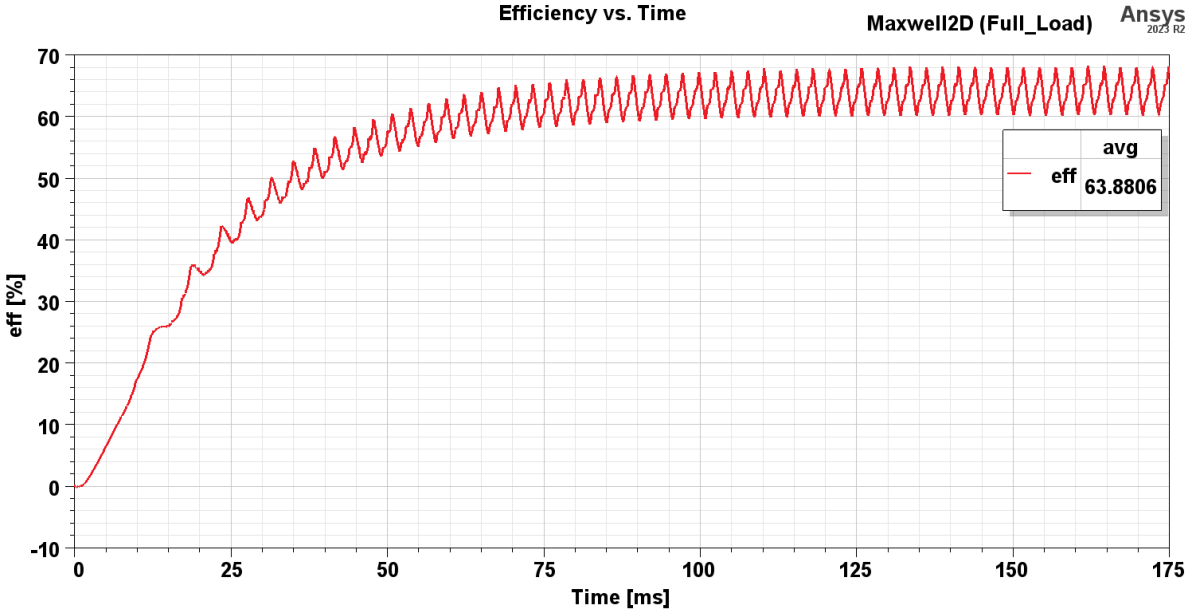

Fig. 29 Efficiency of PMDC Motor at Full Load by Maxwell 2D.

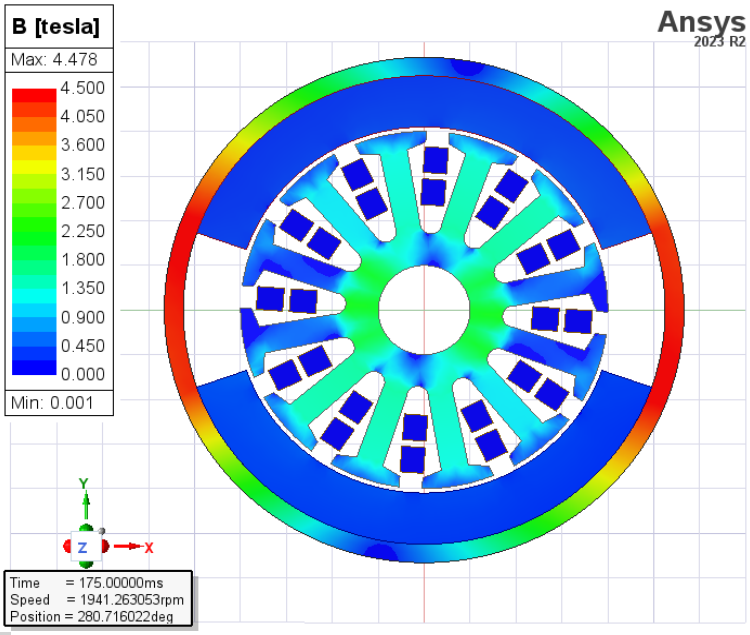

Fig. 30 Magnetic Flux Density Distribution of a PMDC Motor by Maxwell 2D.

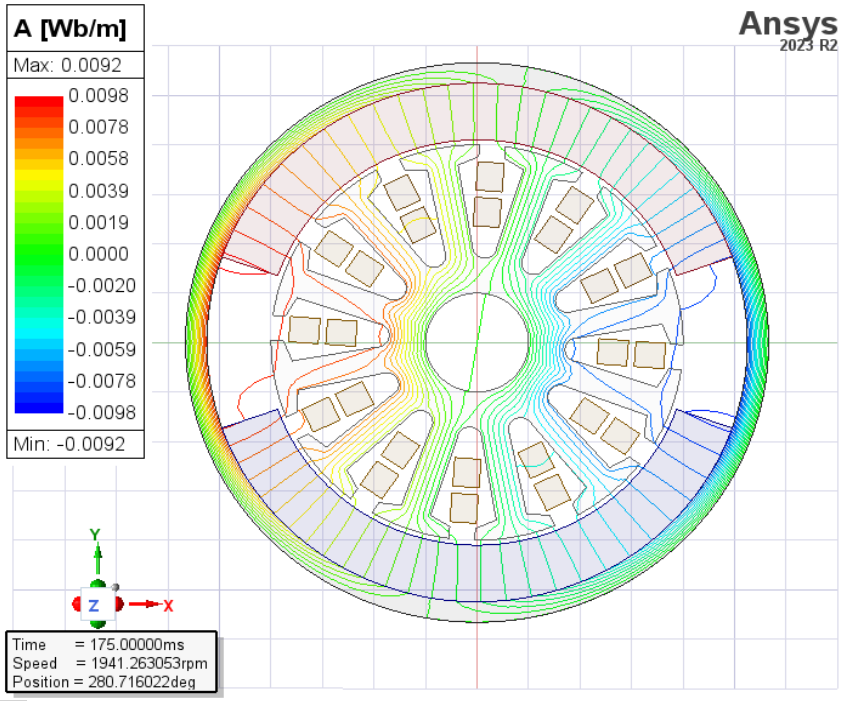

Fig. 31 Electromagnetic Field lines Distribution of a PMDC Motor by Maxwell 2D.

Table 10 Comparison Between Test and RMxprt Results.

Parameter	Unit	Experiment test	RMxprt	Error%
Speed	rpm	1944	1908.51	1.826
Input Current	A	6.42	6.5395	-1.861
Torque	N · m	0.2456	0.2503	-1.914
Input Power	W	77.04	78.4745	-1.862

Table 11 Comparison Between Test and Maxwell2D (Simulation) Results.

Parameter	Unit	Experiment test	Maxwell2D (Simulation)	Error%
Output Power	W	50	50.8973	-1.8
Voltage	V	12	12	0
No-load Speed	rpm	3240	2699.51	16.68
Rated Speed	rpm	1944	1941.2631	0.14
Input Current	A	6.42	6.5029	-1.29
Torque	N · m	0.2456	0.2535	-3.22
Input Power	W	77.04	78.0996	-1.375
Efficiency (%)	%	64.9	63.8806	1.57

Table 12 Comparison of Efficiency and Motor Losses Calculated by RMxprt and Maxwell 2D.

Parameter	Unit	RMxprt	Maxwell 2D	Error%
Armature copper loss (p_{cu})	W	21.2691	21.1506	0.557
Mechanical losses (P_{mech})	W	0.643854	0.6672	-3.626
Core Loss	W	1.02483e-5	0	100
Brush Loss (P_B)	W	6.5395	6.5029	0.56
Stray loss	W	NA	0.781	
Total Loss	W	28.4525	29.102	-2.283
Efficiency (%)	%	63.743	63.8806	-0.216

5.CONCLUSIONS

The current research successfully modeled a specialized PMDC motor for operating automobile windshield wipers using RMxprt/Maxwell 2D, despite the absence of its design information, which was provided through reverse engineering. Maxwell 2D software compared the motor's FEM with RMxprt's analytical results. The results of the lab test were close to each other. Speed, torque, input current, and input power were calculated, as were the losses from which the efficiency was calculated. The hybrid methodology's success in analyzing this motor paves the way for its application in analyzing other motors.

ACKNOWLEDGEMENTS

The authors would like to thank the Electrical Engineering Department, College of Engineering, Mustansiriyah University, Baghdad, Iraq.

REFERENCE

[1] Chun KH, Seo YT, Bae SH, Oh CS. **Characteristics Analysis on Teeth Width of Permanent Magnet DC Motor**. *Proceedings of the KIEE Conference*; 2000.

[2] Lucas O, Patrick C, Mateus G. **Simulation Using FEM for Design PMDC Motors**. *SIMMEA* 2018; Paper 34.

[3] Zaki A, Ibrahim S. **Modeling and Analysis of PM Brushed DC Motor Using FEM**. *2005 European Conference on Power Electronics and Applications*; 2005.

[4] Wing M, Gieras JF. **Calculation of the Steady State Performance for Small Commutator Permanent Magnet DC Motors: Classical and Finite Element Approaches**. *IEEE Transactions on Magnetics* 1992; **28**(5): 2067–2071.

[5] Craiu O, Dan N, Badea EA. **Numerical Analysis of Permanent Magnet DC Motor Performances**. *IEEE Transactions on Magnetics* 1995; **31**(6): 3500–3502.

[6] Karnavas YL, Chasiotis ID, Peponakis ED. **Optimization of Standard PMDC Motors Used in Automotive Applications for Higher Power Density**. *2016 Third International Conference on Mathematics and Computers in Sciences and in Industry (MCSI)*; 2016.

[7] Guzmán H, Ortigoza RS, Sakanassi JO. **Energy-Based Control of Electromechanical Systems**. Cham, Switzerland: Springer; 2021.

[8] Malyar V, Havdo I. **Mathematical Model of Permanent Magnet Direct Current Motor**. *Computational Problems of Electrical Engineering* 2015; **5**(1): 33–36.

[9] Lujara NK. **Loss Modeling of a Permanent Magnet DC Motor Drive Water Pumping System**. *Tanzania Journal of Engineering and Technology* 2017; **35**(2): 84–96.

[10] Chapman SJ. **Electric Machinery Fundamentals**. McGraw-Hill Higher Education; 2005.

[11] Boules N. **Design Optimization of Permanent Magnet DC Motors**. *IEEE Transactions on Industry Applications* 1990; **26**(4): 786–792.

[12] Aslan M, Özpolat AB, İşçi C, Eroğlu F, Vural AM. **Design and Modelling of Internal Permanent Magnet Motor**. *The International Journal of Energy and Engineering Sciences* 2020; **5**(2): 80–104.

[13] Gieras JF. **Permanent Magnet Motor Technology: Design and Applications**. CRC Press, Taylor and Francis Group; 2010.

[14] Bardan HA, Ali AM. **Losses Estimation of Switched Reluctance Motor**. *2023 Second International Conference on Advanced Computer Applications (ACA)*; 2023.

[15] Vladimir K. **Ansoft RMxprt Application Note - A Permanent Magnet DC Motor Problem**. 2011. Available from: https://pdfcoffee.com/a-permanent-magnet-dc-motor-problem-pdf-free.html.

[16] Lehikoinen A, Silwal B, Shah SB. **Efficiency of an Electrical Machine in Electric Vehicle Application**. *Journal of the Institute of Engineering* 2016; **11**(1): 20–29.

[17] Kumar A, Gandhi R, Wilson R, Roy R. **Analysis of Permanent Magnet BLDC Motor Design with Different Slot Type**. *2020 IEEE International Conference on Power Electronics, Smart Grid and Renewable Energy (PESGRE2020)*; 2020; pp. 1–6.

[18] Niruba K, Boopathi S. **Advanced Power Window Motor Using Permanent Magnet DC Motor**. *2014 Power and Energy Systems: Towards Sustainable Energy*; 2014.

[19] Singh VK, Marwaha S, Singh AK. **Design and Analysis of Permanent Magnet Brushless DC Motor for Solar Vehicle using ANSYS Software**. *International Journal of Engineering Research & Technology (IJERT)* 2017; **6**(4): 1215–1220.

[20] Rahman NNA, Yahya NM. **A Mathematical Model of a Brushed DC Motor System**. *Data Analytics and Applied Mathematics (DAAM)* 2021; **1**(1): 60–68.

[21] Hamdi MA, Jumaa FA. **Improve the Efficiency of Brushless Permanent Magnet DC Motor by ANSYS–MAXWELL 3D/2D**. *Journal of Survey in Fisheries Sciences* 2023; **10**(3S): 3031–3039.

[22] Bardan HA, Ali AM. **Analysis of Switched Reluctance Motor Based on RMxprt, Maxwell2D and Matlab**. *2022 2nd International Conference on Advances in Engineering Science and Technology (AEST)*; 2022; pp. 675–680.

[23] Almubaidin MA, Ahmed AN, Winston CAA, El-Shafie A. **Application of Machine Learning for Daily Forecasting Dam Water Levels**. *Tikrit Journal of Engineering Sciences* 2023; **30**(4): 74–87.

[24] Jategaonkar A, Lenin NC. **Electromagnetic Analysis of Permanent Magnet Brushed DC Motor for Automotive Applications—Part 1**. SAE Technical Paper; 2021.

[25] Özüpak Y. **Design and Analysis of Permanent Magnet DC Machines with FEM Based ANSYS-MAXWELL**. *International Journal of Innovative Engineering Applications* 2023; **7**(1): 7–12.

[26] Jassim AH, Hussein AA, Abbas LF. **The Performance of a Three-Phase Induction Motor Under and Over Unbalance Voltage**. *Tikrit Journal of Engineering Sciences* 2021; **28**(2): 15–32.

[27] Aslan M, Özpolat AB, İşçi C, Eroğlu F, Vural AM. **Design and Modelling of Internal Permanent Magnet Motor**. *The International Journal of Energy and Engineering Sciences* 2020; **5**(2): 80–104.

[28] Nandhakumar A, Santhoshkumar KV, Raja TA, Sonaa JCR, Kavya S, Swetha S. **Design and Analysis of Brushless DC Motor for Pure Electric Vehicle**. *International Journal of Electrical Engineering and Technology* 2022; **13**(5): 19–25.

[29] Chen GR, Hsiao HC, Hsiao CY. **Three-Dimensional Finite-Element Analysis and Optimal Design of Hybrid-Excitation DC Brush Motor for Automotive Engine Start Applications**. *IEEJ Journal of Industry Applications* 2023; **12**(1): 65–72.

[30] Rahman NNA, Yahya NM. **A Mathematical Model of a Brushed DC Motor System**. *Data Analytics and Applied Mathematics (DAAM)* 2021; **1**(1): 56–62.